Journal of Enzyme Inhibition and Medicinal Chemistry, 2011; 26(6): 871–882

ISSN 1475-6366 print/ISSN 1475-6374 online
DOI: 10.3109/14756366.2011.557023

informa
healthcare

ORIGINAL ARTICLE

Design, synthesis, and biological evaluation of bifunctional thyrointegrin inhibitors: new anti-angiogenesis analogs

Alexandre Bridoux[1,2], Riaz A. Khan[1,3], Celei Chen[1], Gwenaël Chevé[4], Huadong Cui[1], Evgeny Dyskin[1], Aziz Yasri[4], and Shaker A. Mousa[1,2,5]

[1]Pharmaceutical Research Institute, Rensselaer, NY, USA, [2]Vascular Vision Pharmaceuticals, Rensselaer, NY, USA, [3]Department of Chemistry, Manav Rachna International University (MRIU), Faridabad, Haryana, India, [4]NOVADECISION, Rond point Benjamin Franklin–C539521, 34950 Montpellier Cedex 2, France, and [5]King Saud University, Riyadh, Kingdom of Saudi Arabia

Abstract

Context: Inhibition of pathological angiogenesis.

Objective: Obtaining new transactivator, bifunctional, thyroid antagonist, non-toxic anti-angiogenic compounds.

Materials and methods: *In silico* drug design, synthesis in bulk and biological evaluation in chick chorioallantoic membrane (CAM) model.

Results: Significant inhibition (range 65–73%) at 0.25–2.0 μg/ml doses.

Discussion and conclusion: The synthesis of compounds (**9**), (**10**), and (**11**) incorporating long-chain moieties guanidine, urea, methyl amine and, propyl amine substitutions, respectively, into the core molecular framework of tetrac (tetraiodothyroacetic acid) were undertaken. The evaluation of the anti-angiogenic bioactivity of these compounds in the CAM model revealed no loss of activity in comparison with tetrac and XT199, which showed nearly 86% inhibition at dose levels of 1 and 0.5 μg/ml, respectively, and validated the concept.

Keywords: Antiangiogenesis, XT199, dual thyrointegrin antagonist, molecular modelling, chick chorioallantoic membrane assay

Introduction

Integrins are transmembrane, obligate, and heterodimeric receptor proteins consisting of α and β chain units[1–4]. On binding of a ligand to a specific recognition site in the extracellular domains of the integrin receptor αVβ3, identified as Arginine-Glycine-Asparagine (RGD) recognition site, the multicomponent signalling complexes are activated via specific protein–protein interactions of the cytoplasmic tail of the receptor with various signal transduction molecules. The action of mitogen-activated protein kinase (MAPK) signalling cascade is one of the earliest events following ligand–receptor binding[5–8]. Through the activation of diverse signalling pathways, including MAPK, the integrins also regulate a variety of biological processes, including cell differentiation, wound-healing, and apoptosis[9–12]. The integrin receptors play an important role in cell–cell signalling by mediating interactions between cells and, attachment of cells to the extracellular matrix, thus, helping to define the cellular shape, cell motility regulation, and modulation of cell cycle progressions[13–16]. Integrins also play a critical role in angiogenesis, a complex biological process of new blood vessel formation that involves local release of vascular growth factors, interactions between adjacent and far-off cells, the extracellular matrix, and modulation of biochemical and other metabolic processes[17]. The integrins αVβ3 and αVβ5 are the main receptor types involved in angiogenesis[18,19]. One of the ways that tumours respond to

Address for Correspondence: Shaker A. Mousa, Ph.D., MBA, FACC, FACB, Professor of Pharmacology and Executive Vice President, Chairman of the Pharmaceutical Research Institute at Albany, Albany College of Pharmacy and Health Sciences, 1 Discovery Drive (Room 238), Rensselaer, NY 12144. E-mail: Shaker.Mousa@acphs.edu

(Received 09 September 2010; revised 04 January 2011; accepted 18 January 2011)

damage induced by chemotherapy or other means is by expressing and secreting biochemical factors that protect the tumour vasculature, including integrin receptors[20]. In addition, tumour growth, resistance to chemotherapy, and metastasis, all involve integrin-mediated cellular and extracellular signalling pathways, wherein the up-regulation of integrin αVβ3 expression serves as an escape mechanism for tumours[21,22]. One of the ways to control the tumour progression has been to control angiogenesis via integrin antagonists[23–27]. The integrin antagonists that function effectively as anti-angiogenic agents were identified earlier[28]. The arginine-glycine-aspartate (RGD), cyclic RGD tripeptide (c-RGD) (Figure 1) and c-RGD peptidomimetics have been shown to be effective integrin αVβ3 antagonists as well[29,30]. The c-RGD exhibited enhanced antiangiogenic and antitumour activities in radiation and chemotherapy led studies in tumours[31,32]. Results of recent studies[33,34] suggest that in addition to integrin antagonists, the thyroid antagonists could also modulate angiogenesis. Several other reports[35–38] have described the effects of thyroid hormone analogs on integrin αVβ3, thyroid hormone receptor, and membrane Na^+/H^+ anti-porter ion pumps, revealing a complex relationship between thyroid hormone and nuclear events that underlie important cellular and tissue processes, including angiogenesis and tumour cell proliferation. The thyroidhormone analogs, 2-ammonium-3-[4-(4-hydroxy-3-iodophenoxy)-3,5-diiodophenyl]-propionate (T_3) and 2-ammonium-3-[4-(4-hydroxy-3,5-diiodophenoxy)-3-,5-diiodophenyl] propionate (T_4), have been shown to induce angiogenesis[39,40], while the metabolic degradation product of thyroid hormone, tetra-iodothyroacetic acid (tetrac), inhibits angiogenesis in the chick chorioallantoic membrane (CAM) and other angiogenesis models (Figure 1)[41–45]. Thus, tetrac, which is a deaminated derivative of T_4, serves as a thyroid antagonist by blocking the actions of T_3 and T_4. Interestingly, c-RGD and other small molecule c-RGD peptidomimetics also inhibit the activation of MAPK, an early signalling event that is required for angiogenesis. These results indicate that the thyroid hormone interaction site is located at or near the RGD recognition site on integrin αVβ3 receptor. Thus, ligands that block this site would function both as a thyroid and an αVβ3 integrin receptor antagonist. The examples of blocking of iodothyronine binding to the integrin αVβ3 receptor site by tetrac results in the growth arrest of glioma cells[46–51] and human breast cancer cells *in vitro*[18,52–55] that has led to infer that desirable neovascularization could be promoted with local application of thyroid hormone analogues during wound healing, and the undesirable angiogenesis that supports tumour growth, could be arrested with tetrac or its structurally related derivatives.

Tetrac and tetrac analogs, through their activity at the integrin αVβ3 receptor binding site for thyroid hormone, inhibit angiogenesis and have been shown[56] to modulate proliferation of drug-sensitive and drug-resistant cells, e.g., human neuroblastoma SKN-SH cells, osteogenic sarcoma SaOS2 cells, and human breast adenocarcinoma MCF7 cells. Because of its ability to reverse the poor response of cancer cells to chemotherapy and reduce the proliferation of drug-resistant tumours, tetrac represents not only a biological tool for modulating thyroid hormone action but also a prospective anti-cancer agent that functions as a dual action thyroid hormone and αVβ3 integrin receptor antagonist. Herein, rational drug design was used to generate compounds that were capable of suppressing angiogenesis and, thereby potentially inhibiting tumour growth by suppressing undesirable angiogenesis in the tumour environment and also function as thyroid antagonists. The structural analogs of tetrac with bifunctional biological activity as transactivated thyroid and integrin αVβ3 antagonists were designed by molecular modelling[57,58] program FlexX v3.1.2 BioSolveIT GmbH (Sankt Augustin, Germany) at the thyroid and integrin sites identified by respective ligands, i.e., tetrac and XT199 (Figure 1) *in silico* at the

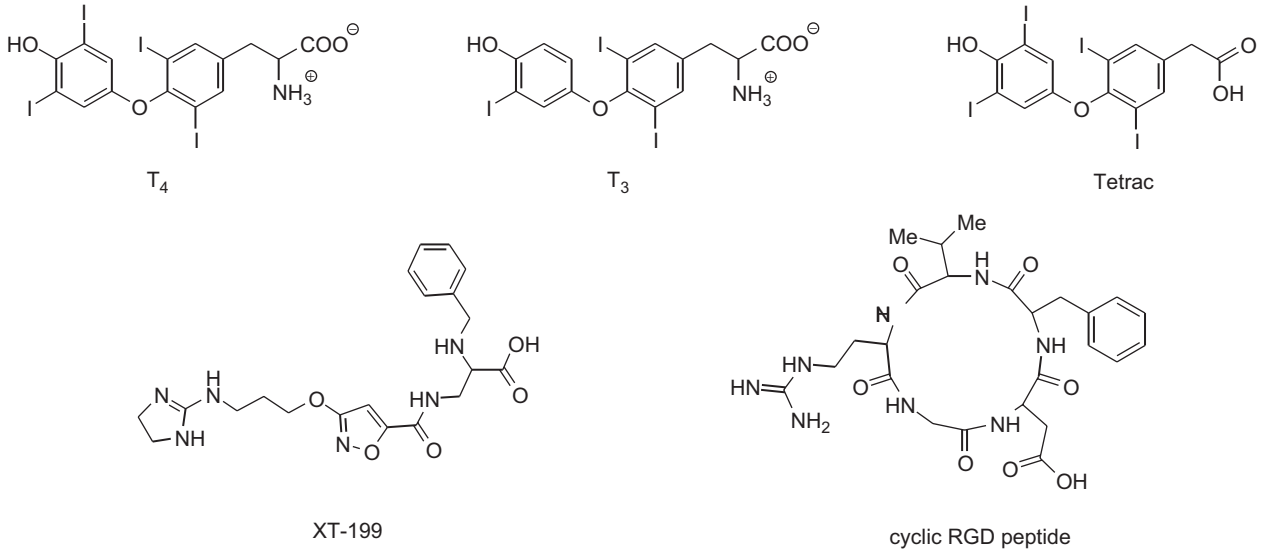

Figure 1. Structures of T_4, T_3, Tetrac, XT199, and cyclic RGD tripeptide.

integrin αVβ3 receptor site. The simulated *in silico* binding of designed compounds and their virtual anti-angiogenic binding profiles in live biological systems corroborated the bifunctional nature of the RGD and c-RGD led receptor sites[59]. Several theoretical compounds were generated in the *in silico* molecular modelling using tetrac and the selective αVβ3 integrin antagonist XT199 as starting templates. The compounds with similar binding characteristics and nearly identical structures and physico-chemical properties were synthesized. The target compounds exhibited pronounced anti-angiogenic activity in the CAM model of angiogenesis in the bioevaluation process.

Methods

All commercially available chemicals were used without further purification. All solvents were dried, and moisture-sensitive reactions were performed under dry nitrogen. Analytical thin layer chromatography (TLC) was performed on precoated Kieselgel $60F_{254}$ plates Merck (Gibbstown, NJ). Analytical Reverse Phase Thin Layer Chromatography (RPTLC) was performed on precoated Kieselgel plates (Merck). Compounds were visualised by ultraviolet (UV) and/or with iodine. Column chromatography was performed with silica gel Kieselgel Si 60, 0.040–0.063 mm (Merck). Melting points were determined on an Electrothermal MEL-TEMP® melting point apparatus and then on a Thomas Hoover Uni-melt capillary melting point apparatus and were not corrected. The structures of all compounds were supported by infrared spectra recorded on a Thermo Electron Nicolet Avatar™ 330 Fourier transform infrared apparatus. UV spectra were obtained from a Shimadzu UV-1650 (PC) UV–vis spectrophotometer. ^{1}H NMR data were obtained using a Varian Inova™ 500 MHz spectrometer and referenced to $CDCl_3$ ($\delta = 7.27$ ppm) or DMSO-d_6 ($\delta = 2.50$ ppm). High-resolution mass spectral analyses were obtained on either Applied Biosystems API4000™ LC/MS/MS or Applied Biosystems QSTAR® XL mass spectrometers. ^{1}H NMR chemical shifts were reported in parts per million downfield from tetramethylsilane, *J* values were in Hertz and the splitting patterns were designated as follows: s, singlet; d, doublet; dd, doublet of doublets; t, triplet; q, quartet; m, multiplet; b, broad. High pressure liquid chromatography (HPLC) experiments were carried out at a flow rate of 1.1 mL/min with a Waters™ 2695 HPLC apparatus (120 vials) and a Phenomenex Luna® 5u NH_2 100A or a Waters μBondapak® C18 10 μm 125A column operated at 40°C and atmospheric pressure with UV detection between 210 and 400 nm. Refractive index was measured with an Abbe 3L Refractometer with bromonaphtalene as the contact liquid. Combustion analyses were performed by Intertek, Inc, Whitehouse, NJ. The yields quoted in this study were recrystallization yields.

Molecular modelling

Lock and key model[57] was used to investigate ligand-binding model behaviour at αVβ3 integrin receptor macromolecular structure site. The DOCK and Autodock that modulates and characterize ligand–integrin interplay at the atomic level were used wherein Autodock was programmed to allow torsional flexibility in ligands to optimize the ligand binding, whereas DOCK was pre-set with a different set of algorithm to match common points located within the binding site and incoming ligands. The simulated docking of known ligand RGD, tetrac, and its antagonistic analogue XT199 to integrin αVβ3 receptor was performed using FlexX version 3.1.2 (BioSolveIT GmbH). The three-dimensional crystal structure of the extracellular segment of integrin αVβ3 in conjunction with the known cyclic peptide ligand RGD was obtained from the Protein Database (PDB: 1L5G).

The active site was identified as a pocket consisting of all amino acids residual atoms within 15 Å radius of the cyclic peptide ligand. The peptide ligand was then removed but three locations of manganese ions were retained, as they participate in the test-template bindings. The receptor was not further modified and treated as a rigid entity during all docking experiments for all test templates. Since the FlexX (v3.1.2) uses incremental construction, each test compound was before-hand fragmented into smaller components and reconstructed sequentially within receptor cavity for docking. The qualitative interactions for the first fragment were identified followed by estimation for the target compound by joining the remaining components in a step-wise manner. After addition of each component, the new interactions were defined, and scoring function was used to select the best partial solution. This was repeated until reconstruction of the original ligand was fully achieved. Of the 30 different solutions generated by FlexX, the best one was chosen based on FlexX score and best optimal position within the active site.

Synthesis of compounds

[4-(4-Hydroxy-3, 5-diiodophenoxy)-3, 5-diiodophenyl] acetic acid (6)

The title compound was prepared as described by Wilkinson[60].

Methyl [4-(4-hydroxy-3,5-diiodophenoxy)-3,5-diiodophenyl] acetate (7)

[4-(4-Hydroxy-3, 5-diiodophenoxy)-3,5-diiodophenyl] acetic acid (5.0 g, 6.7 mmol, 1.0 equiv.) was dissolved in 200 mL of dried MeOH and thionyl chloride (485 μL, 6.7 mmol, 1.0 equiv.) was added dropwise. The reaction was refluxed for 2 days. After the completion of the reaction, water was added (200 mL) and concentrated to ½ (or till precipitate appeared) which was collected by filtration and dried. The solid thus obtained was crystallized from EtOH to yield the desired product as white powder. Yield: 100%; TLC: Rf = 0.81 (DCM); RPTLC: Rf = 0.49 ($AcOH/H_2O$ 90/10); mp = 163°C; IR (cm^{-1}): 1719 (characteristic peak); UV (DMSO): λ_{max} 225 nm; HPLC (μBondapak C18): rt 3.2 minutes ($MeOH/H_2O$ 65/35); ^{1}H NMR ($CDCl_3$): 7.78 (s, 2H, ArH), 7.12 (s, 2H, ArH), 3.75 (s, 3H, CH_3), 3.58 (s, 2H,

CH_2); ^{13}C NMR ($CDCl_3$): 152.8, 150.2, 149.6, 142.3, 135.2, 126.9, 125.3, 91.0, 81.9, 52.3, 39.3; HRMS (APCI) *m/z*: 760.8904 [$(M–H)^-$, 5%].

Methyl {4-[4-(2-chloroethoxy)-3,5-diiodophenoxy]-3,5-diiodo phenyl}-acetate (8)

Methyl [4-(4-hydroxy-3,5-diiodophenoxy)-3,5-diiodophenyl]acetate (**7**, 2.4 g, 3.2 mmol, 1.0 equiv.) was dissolved in anhydrous acetone, cesium carbonate (522 mg, 1.6 mmol, 0.5 equiv.), followed by 1-bromo-2- chloroethane (275 µL, 3.2 mmol, 1.0 equiv.) were added dropwise and after stirring over 3 days at room temperature (RT), the reaction medium was Celite-assisted filtered and filtrate evaporated to give a yellow solid that was crystallized from EtOH to give white product. Yields: 100%, TLC: Rf 0.76 (CH_2Cl_2); mp 119°C; IR (cm^{-1}): 1732 (characteristic peak); UV (DMSO): max = 256 nm; HPLC (µBondapak C18): rt 4.7 min (MeOH/H_2O 70/30); ^1H NMR ($CDCl_3$): 7.75 (s, 2H, ArH), 7.15 (s, 2H, ArH), 4.19 (t, *J* = 5.5 Hz, 2H, CH_2), 3.91 (t, *J* = 5.5 Hz, 2H, CH_2), 3.72 (s, 3H, CH_3), 3.55 (s, 2H, CH_2); HRMS (APCI) *m/z*: 823.6 [(M)+, 100%]; Elem. Anal. ($C_{17}H_{13}ClO_4I_4$) C: calcd, 24.77; found, 24.98, H: calcd, 1.59; found, 1.52.

Lithium [4-(4-{2-[(diaminomethylene) amino]-ethoxy}-3,5-diiodophenoxy)-3,5-diiodophenyl] acetate (9)

To a solution of methyl {4-[4-(2-chloroethoxy)-3,5-diiodophenoxy]-3,5-diiodophenyl}acetate (**8**, 200 mg, 0.2 mmol, 1.0 equiv.) in anhydrous N,N'-dimethylformamide (DMF) (5.0 mL) was added sodium hydride (60% dispersion in mineral oil; 19 mg, 0.5 mmol, 2.0 equiv.) in portions followed by 10% guanidine hydrochloride (46 mg, 0.5 mmol, 2.0 equiv.) in dry DMF (5.0 mL) and RM stirred for 12 h at RT. After the completion of reaction monitored by TLC, the RM was treated with LiOH solution (115 mg, 4.9 mmol, 20.0 equiv.) and precipitate obtained was filtered, dried, and crystallized from EtOH to give white powder. Yield: 50%, TLC: Rf 0.12 (EtOH); mp 133°C; IR (cm^{-1}): 1736 (characteristic peak); UV (DMSO): λ_{max} 256 nm; HPLC (µBondapak C18): rt 6.1 minutes (MeOH/H_2O 65/35); ^1H NMR (CD_3OD): 7.88 (s, 2H, ArH), 7.19 (s, 2H, ArH), 4.20 (t, *J* = 5.5 Hz, 2H, CH_2), 3.91 (t, *J* = 5.5 Hz, 2H, CH_2), 3.45 (s, 2H, CH_2); ^{13}C NMR ($CDCl_3$): 206.9, 171.5, 153.2, 152.7, 151.8, 141.5, 136.7, 126.0, 92.0, 91.8, 72.9, 52.3, 43.8, 38.1; HRMS (APCI) *m/z*: 841.7599 [(M+3H+Li)+, 100%].

(4-{4-[2-(Carbamoylamino)ethoxy]-3,5-diiodophenoxy}-3,5-diiodophenyl) acetic acid (10)

To a solution of methyl {4-[4-(2-chloroethoxy)-3,5-diiodophenoxy]-3,5-diiodophenyl}acetate (**8**, 1.5 g, 1.8 mmol, 1.0 equiv.) in anhydrous DMF (15.0 mL) was added sodium hydroxide (285 mg, 7.1 mmol, 4.0 equiv.) by portions followed by urea solution (107 mg, 1.8 mmol, 1.0 equiv.) in anhydrous DMF (5.0 mL) and RM was stirred for 10 h at RT. After the completion of reaction monitored by TLC, the RM was treated with a solution of LiOH (504 mg, 21.0 mmol, 12.0 equiv.) and precipitate thus obtained was filtered, dried, and crystallized from hot EtOH as light brown powder. Yields: 50%; TLC: Rf 0.77 (CH_2Cl_2); RPTLC: Rf 0.5 (AcOH); mp 267°C; IR (cm^{-1}): 1735; UV (DMSO): λ_{max} 256 nm; HPLC (µBondapak C18): rt 3.85 minutes (MeOH/H_2O 60/40); ^1H NMR (CD_3OD): 7.88 (s, 2H, ArH), 7.19 (s, 2H, ArH), 4.19 (t, *J* = 5.5 Hz, 2H, CH_2), 3.95 (t, *J* = 5.5 Hz, 2H, CH_2), 3.45 (s, 2H, CH_2); HRMS (APCI) *m/z*: 834.5700 [(M+H)+, 34%]; Elem. Anal. ($C_{17}H_{14}I_4N_2O_5$) C: calcd, 24.48; found, 24.57; H: calcd, 1.69; found, 1.59.

{4-[4-(3-Aminopropoxy)-3,5-diiodophenoxy]-3,5-diiodo phenyl} acetic acid (11)

To a solution of methyl {4-[4-(2-chloroethoxy)-3,5-diiodophenoxy]-3,5-diiodophenyl}acetate (**8**, 2.5 g, 3.3 mmol, 1.0 equiv.) in cyclopentyl methyl ether (20.0 mL), Et_3N (460 µL, 3.3 mmol, 1.0 equiv.), chloropropylamine (427 mg, 3.3 mmol, 1.0 equiv.) was added and RM was refluxed for 3 h, followed by solvent evaporation to a minimum volume. Water was added to the residual material, which was further treated with LiOH solution (1.6 g, 66.0 mmol, 20.0 equiv.) to give a precipitate that was collected after filtration and dried to give a powdery solid. The obtained powder was washed *under vacuuo* with warm MeCN followed by warm EtOH and dried to give a solid that was further dissolved in anhydrous EtOH (5.0 mL) and a solution of HCl 0.1 N (5.0 mL) was added dropwise to give a precipitate, which after filtration was obtained as a white powder (668 mg) to which NaOH (280 mg, 6.6 mmol, 2.0 equiv.) as aqueous solution was added under stirring, this solid suspension was filtered, dried, and crystallised in EtOH to give a white powder. Yield: 47%, mp 250°C; IR (cm^{-1}): 1697; UV (DMSO): λ_{max} 259 nm; HPLC (µBondapak C18): rt 17.5 minutes (ammonium acetate 25mM pH4/MeOH 50/50); ^1H NMR (Acetone-d6): 7.99 (s, 2H, ArH), 7.30 (s, 2H, ArH), 4.27 (t, *J* = 5.5 Hz, 2H, CH_2), 3.95 (t, *J* = 5.5 Hz, 2H, CH_2), 3.75 (s, 2H, CH_2), 3.57 (q, *J* = 14.0 Hz, *J* = 7.0 Hz, 2H, CH_2); HRMS (APCI) *m/z*: 832.6368 [(M–2H+Li+Na)+, 100%]; HRMS (APCI) *m/z*: 764.7010 [$(MCOOH+Li)^-$, 100]; 'Elem. Anal. ($C1_7H_{14}I_4LiNO_4$) C: calcd, 25.18; found, 24.87; H: calcd, 1.74; found, 1.53.

2-Isopropyl anisole (13)

The title compound was prepared with minor variations from the protocol described by Baxter et al.[61]. Yield: 60%, yellow oil; TLC: Rf 0.65 (cyclohexane-EtOAc (95:5)); ^1H NMR ($CDCl_3$): 7.32–7.30 (dd, *J* = 8.0 Hz, 2.5 Hz, 1H, ArH), 7.27–7.23 (dt, *J* = 9.5 Hz, 2.0 Hz, 1H, ArH), 7.04–7.01 (dt, *J* = 7.5 Hz, 1.0 Hz, 1H, ArH), 6.94–6.92 (dd, *J* = 8.0 Hz, 1.0 Hz, 1H, ArH), 3.90 (s, 3H, CH_3), 3.47–3.41 (m, 1H, CH), 1.30 (s, 3H, CH_3), 1.20 (s, 3H, CH_3); $n[D]_{20}$ 1.5069.

bis[4-methoxy-3-(propan-2-yl)phenyl]iodonium tetrafluoroborate (14)

The title compound was prepared as described by Yokoyama et al.[62]

Methyl (3, 5-di-tert-butyl-4-hydroxyphenyl) acetate (16)

To 2,6-di-*tert*-butyl-4-hydroxyphenylacetic acid (15.0 g, 56.7 mmol; 1.0 equiv.) dissolved in 100 mL of dried MeOH was added thionyl chloride (4.1 mL; 56.7 mmol; 1.0 equiv.) in a dropwise manner and RM refluxed for 50 h. After completion of the reaction, monitored by TLC, water was added (200 mL) and RM was concentrated to one-third volume to give a precipitate that was collected by filtration and extracted from water with the EtOAc organic phase after evaporation and drying of the solvent (total 20 g). The solid was crystallised in EtOH, filtered, and washed with cold EtOH to give transparent crystals. Yield: 100%; mp: 88°C; TLC: Rf 0.81 (CH_2Cl_2); RPTLC: Rf 0.78 (AcOH); IR (cm^{-1}): 1722; UV (DMSO) λ_{max} 276 nm; HPLC (μBondapak C18): rt 4.0 min (MeOH/H_2O 65/35); ^1H NMR ($CDCl_3$): 7.14 (s, 2H, ArH), 3.75 (s, 2H, CH_2), 3.60 (s, 2H, CH_2), 1.50 (s, 18H, CH_3); ^{13}C NMR ($CDCl_3$) 172.9, 153.2, 136.2, 126.9, 125.3, 124.9, 53.3, 51.7, 51.0, 41.2, 40.1, 34.5, 32.4, 31.2, 29.9, 28.5; Elem. Anal. ($C_{17}H_{26}O_3$) C: calcd, 73.34; found, 73.39; H: calcd, 9.41; found, 9.27.

Biological assays

The compounds were tested in the CAM model[43–45] wherein 10 day old fertilized chicken eggs, eight per treatment (Sunrise Farms Inc., Catskill, NY) were incubated at 37°C with 55% relative humidity. In dark, with the help of a candling lamp, a small hole was punctured in the area of the shell covering egg-air sac with the help of a hypodermic needle. A second hole was punctured on the wider side of the egg above a vascular area of the embryonic membrane. An artificial air sac was created below the second hole by gently applying *vacuum* to the first hole using a small rubber squeeze bulb. The *vacuum* was caused by the separation of CAM from the egg shell. A small window of approximately 1 cm^2 was cut in the egg shell with the help of a mini drill. The underlying CAM was accessed through this window. Filter disks were cut (filter paper #1; Whatman Ltd (Maidstone, Kent, UK)) and soaked in 3.0 mg/mL cortisone acetate solution (in 95% ethanol) and air-dried under sterile conditions. To induce angiogenesis, sterile filter disks were saturated with Fibroblast Growth Factor (FGF) and placed on the CAM window. For control, disks were saturated with PBS without calcium or magnesium. The window was sealed with Highland Brand transparent tape. After an hour, 10 μL of the compound was applied topically to the FGF-stimulated CAM. After a period of 48 h, the CAM tissue beneath the filter disk was harvested for evaluation of angiogenesis. The affected CAM in petri dishes were examined using a SV6 stereomicroscope (Carl Zeiss MicroImaging, Inc.,(Thornwood, NY) and Media Cybernetics, Inc. (Bethesda, MD)) at 50× magnification and the images were captured using a 3-CCD colour digital video camera (Toshiba America Inc., New York, NY). The images were analyzed using Image-Pro Plus program (Media Cybernetics, Inc). The numbers of branch points in samples within a circular region superimposed on the area of the filter disk were counted for each treatment condition. Stock solutions of compounds (**9**), (**10**), and (**11**) of 1.0 mg/mL and 1.2 μM were diluted to a final concentration of 0.25 mg/mL or 0.3 μM and the two concentrations for each compound were tested. XT199 (10.0 μM), a synthetic avβ3 antagonist developed at DuPont Pharmaceuticals, and tetrac (1.0 μM) were tested as references and compared with synthesized designed products. Ten microliters of each test solution was added to the filter disks pretreated with FGF as described earlier. All the compounds exhibited strong anti-angiogenic activity with an average of 63–75% inhibition at 0.3 μM dose levels.

Statistical methods

Statistical analyses were performed using ANOVA, software Statview (Adept Scientific, Acton, MA) and SigmaPlot (version 10.0, Systat software Inc., Chicago, IL). The mean ± SEM of branch points and the concentration of haemoglobin from each experimental group were compared with their respective controls. The statistical significances was defined as $P < 0.01$. In the CAM studies, the angiogenesis index for each treatment group were compared with the corresponding control groups.

Results and discussion

The integrin αVβ3 receptor transduces signals through intracellular activation, which induces conformational changes in the targeted receptor that allows extracellular binding of ligand[63]. Cocrystallization studies[64] have revealed the details of the binding interactions of natural ligands to integrin αVβ3 at the molecular levels. These studies reveal that the interface of the propeller region of the αV subunit and the β3A region (the head of the receptor protein) are key regions that participate in the receptor–ligand interaction.

The structures of T_4, T_3, tetrac, XT199, and the cyclic RGD tripeptide are shown in Figure 1. Analysis of the integrin receptor cocrystallized with the cyclic RGD tripeptide provided the starting point for the design process, and templates were based on the molecular characteristics of the α and β units of the receptor and ligand–receptor interaction areas (Supporting information). Structural mapping has provided details of the molecular architecture of the RGD tripeptide bound at the interface of the propeller region of αV and β3A subunits in the head region of integrin αVβ3 receptor[65]. Other modelling studies have confirmed that there is sufficient space in the binding cavity for thyroid hormone constituents to bind. Since thyroid hormone analogs (T_3 and T_4) and tetrac are smaller in overall length than the cyclic RGD tripeptide, they do not interact with the Arg^{214} recognition site in the propeller domain of αV subunit; most of the interactions are confined to the βA subunit domain of the αVβ3 receptor[66].

The linear RGD tripeptide, length-modified RGD as RGDF tetrapeptide and antagonist XT199 occupied a shallow crevice between the αV propeller and β3A subunits located in the integrin upper region on the αV propeller (head) and βA domains exclusively contacting Arg

and Asp amino acids (AA) residues while Asp chelated the metal ion located at a distance of 2.6 Å in the receptor cavity.

The molecular details of the interaction of the cyclic RGD tripeptide were used to dock the primary ligand tetrac (Figure 2A and 2C), XT199 (Figure 2B) and newly designed compounds (Supporting information) to the integrin aVβ3 receptor. For each compound, the carboxylic acid moiety was responsible for the ligand–receptor interaction and was involved in metal ion binding (2.6 Å from the metal ion), which occurs only in the active state of the integrin receptor. For thyroid antagonist XT199, the phenyl sulphonamide moiety stabilized the metal binding through an interaction with Arg^{214}, whereas tetrac interacted with the manganese metal ion and was stabilized by electrostatic interaction with the vicinal Asn^{215} together with hydrogen bonding with the OH of phenol of Tyr^{178}. Of all the compounds examined, XT199 was the only entity with sufficient molecular length to interact with the Arg^{214} recognition site in the propeller region of αV, thus the constituting imidazolyl group in XT199 was found as a best fit between Asp^{150} and Asp^{218} amino acid residues within the binding pocket and paving the way for lengthening of the ligand beyond 13.51 Å as in the case of RGDF. The superimposition of structures of XT199 and the RGD tripeptide showed that the spatial orientation of the entire XT199 molecule was nearly identical to the structure of the RGD tripeptide (Figure 3). The RGDF peptide extends the length of the RGD tripeptide beyond 14.48 Å. The lengths of RGDF and compounds **9**, **10**, and **11** were in the effective binding range lengths of 15.00 Å for the adopted conformations during binding. The adopted geometry of the templates (tetrac and XT199) and the designed compounds **9**, **10**, and **11** contributed positively in binding to the αV/βA region of the integrin receptor. The role of different amino acids in providing hydrogen bonding and interactions within the propeller region of αV subunit for larger length molecules was clearly different than for shorter length molecules, that is, tetrac. This was a further indication of a dual role of the integrin receptor, via both integrin ligand and thyroid binding domains, as a thyrointegrin receptor with transactivation capabilities, and a strong indication that the designed compounds would have bifunctional activity as integrin inhibitors and thyroid antagonists[60,67–73].

The *in silico* binding of the designed compounds and superimposition of their binding orientations with peptide ligands, tetrac, and XT199 antagonist again showed the effective geometry of the compounds **9**, **10**, and **11** to be shorter than those in peptides and XT199 due to the perpendicular twisted geometry of the adjacent phenyl rings linked and manoeuvrable through an ether bond. The fact that the ligands and other molecules with known integrin and thyroid antagonist action bind to different amino acid residues in the same receptor cavity of αVβ3 integrin again suggested an interlinked role for the integrin receptor in modulating angiogenesis and thyroid action.

To design tetrac derivatives that would function as true integrin αVβ3 antagonists, the structure of tetrac was modified using molecular spacers to achieve the required molecular length for *in silico* binding to the αV and βA receptor-binding sites. The structural comparisons of non-peptide integrin antagonists that are active in the nanomolar dose levels[61,74–76] were also evaluated using FlexX to derive compounds **9**, **10**, **11**, and **17**. The functional groups that were altered/affixed to tetrac were selected based on their ability to reach and interact with the Arg^{214} recognition site in the propeller region of the αV subunit. The distance between the carboxylic acid and the amino functional groups was found to be critical for *in silico* binding; thus, we designed molecules with substitutions wherein the distance between these two functional groups was close enough to retain binding to the desired location in the receptor cavity and maintain integrin antagonist activity (Figure 3). The distance between the amino acid and carboxylic acid groups was in agreement with average interpoint atomic distance defined according to a three-point pharmacophore pattern for all incoming templates at the integrin receptor site in conjunction with the observation of the ligand length and size of the receptor cavity. The interpoint atomic distance was estimated by a three-point model delineating 15.00 Å for two sides and a maximum of 7.00 Å for the third and extreme left arm of the triangle. Optimization of structures that were close to the molecular length and geometry of tetrac were carried out to obtain improved

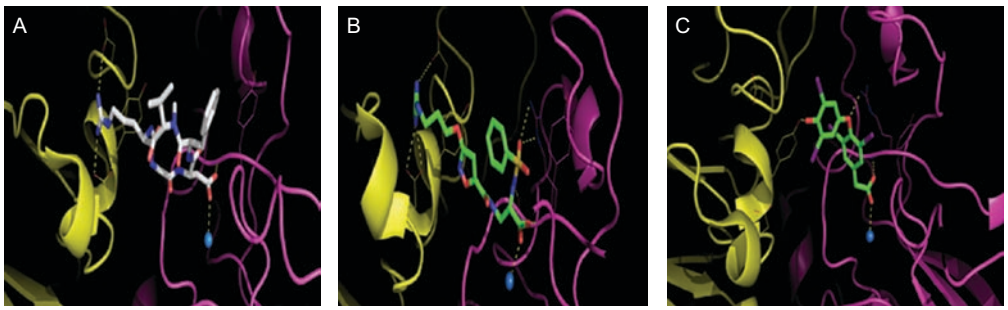

Figure 2. (A) Cyclic RGD tripeptide (white) bound at the interface of αV (yellow) and β3A (purple). The blue ball represents a manganese ion; yellow doted lines represent H-bond interactions (low visibility here). (B) XT199 (green) bound at the interface of the αV and β3A subunits of the αVβ3 integrin; (C) tetrac (green) bound at the interface of the αV and β3A subunits.

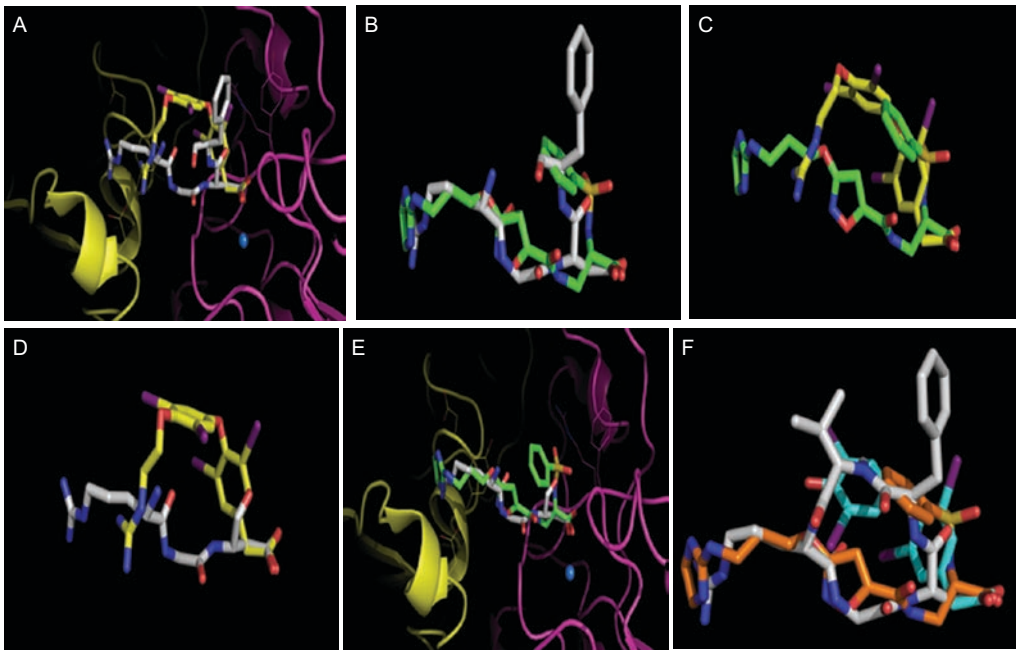

Figure 3. (A) Superimposition of the RGDF tetrapeptide and compound **9**; (B) superimposition of RGDF and XT199; (C) superimposition of XT199 (green) and compound **9** (yellow) revealed slight geometric agreement at CO2H terminal of compound (**9**) in binding mode; (D) superposition of RGD and compound (**9**) revealed slight geometric agreement in binding mode only at CO_2H terminal of compound (**9**); (E) the RGD (white/blue) tripeptide superimposed at common coordinates with XT199 (green) in the bound state at the integrin receptor; (F) superposition of XT199, RGDF and tetrac.

alternatives. On the basis of effective *in silico* binding of the tetrac-derived molecules in the receptor cavity that satisfied all the requirements of thyroid and integrin sites interactions by binding at both the αV and βA domains due to its effective molecular length and physico-chemical characteristics, both iodinated and deiodinated analogs have been generated. The fact that both the thyroid antagonist ligand and integrin receptor-binding (blocking) compounds contained geometric and electronic specifications for binding prompted us also to consider adding high-to-moderate and low electron-rich molecular chain substitutions to tetrac. Due to the presence of the carboxylic acid moiety, responsible for the thyroid antagonist activity-related bindings as observed in the ongoing simulations and which was shown to be crucial for initial receptor and metal binding in the undergoing molecular simulations the OH of phenol of tetrac was selected as the target site for converting tetrac to an integrin antagonist. In line with the observation of binding of different peptides and XT199 ligands *in silico*, the other side (carboxyl end) of the molecule was not modified so as to preserve partial antithyroidal activity.

Estimates of polarizability, refractive index, log P, and molecular volume as well as surface area approximations of tetrac, XT199, cyclic RGD, and compounds **9**, **10**, **11**, and **17** were carried out using Hyperchem (v7.5, Hypercube Inc., Gainesville, FL). Estimated values were nearly identical and in proportion to the designed molecules in accordance with template characteristics (Supporting Information, Table 1). Electrostatic potential, charge density, and distribution in molecules exhibited identical patterns for tetrac, XT 199, RGD, and compounds **9**, **10**, and **11**, as depicted by 2D contour plots and 3D renderings (Figures 4 and 5 and Supporting Information). Estimates of molecular characteristics and analysis of ligand binding to the αVβ3 integrin receptor binding site suggested that the biological activity of deiodinated compound **17** may be in the same range of that of the other compounds (**9**, **10**, and **11**) with only limitation in the geometry of phenyl ring that is hindered from taking a perpendicularly twisted orientation at the receptor site in compound (**17**).

Tetrac (**6**) was synthesized in sufficient quantities for subsequent modification as per synthetic Scheme 1. Appropriate starting material (**1**) was obtained in a two-step process. Commercially available *p*-hydroxy phenylacetic acid was first converted into a dinitro-ester. The nitration reaction, despite the hydroxyl group being favoured for oxidation, occurred in dilute HNO_3 in AcOH with minimum side reactions, contrary to the classical oxidation approach[77] using H_2SO_4, with a moderate yield. Acid-catalyzed esterification of the resulting compound gave the desired intermediate (72% yield), which was then reacted with *para*-toluenesulphonyl chloride and methoxyphenol in pyridine to give the diphenylether derivative (**2**) at a yield of 75%. Catalytic reduction using H_2, 5% Pd and $CaCO_3$ in ethanol as solvent gave product (**3**), which could be tetrazotized in ethanol at 0°C. The *in situ* tetrazolium salt was reacted with NaI to give the 3,5-diiodo derivative (**4**) with a 69% yield[78]. Given the difficulties encountered with aromatic ether hydrolysis of substrate (**4**), complete acidolysis under reflux conditions using hydroiodic acid (HI) as a strong cleaving agent was carried out for facile removal of both the ester

and *O*-methyl groups from product[79,80] (**4**). Acetic acid was used to avoid decomposition of HI into I_2 by H_2SO_4, thereby avoiding the generation of unwanted side products in the reaction medium[78]. Tetrac target molecule (**6**) was obtained from the di-iodo compound (**5**) by reaction with iodine. In the reaction, iodo-deprotonation was carried out using I_2 in methanolic-NH_3 with near quantitative yields. Regioselective iodination of the ring in compound (**5**) was facilitated by the transformation of the methyl ether group of compound (**4**) into an alcohol in substrate (**5**). This was carried out to allow activation of the *ortho* position in compound (**5**) through inductive and resonance effects. Tetrac (**6**) was then esterified in thionyl chloride-MeOH under reflux for 2 days for >60% yield. The hydroxyl group in the resulting compound (**7**) was substituted by 1-chloro-2-bromoethylene C_2H_4BrCl, and the obtained key intermediate (**8**) was then transformed to give the thyrointegrin antagonist compounds (**9**), (**10**)

Table 1. Inhibition of angiogenesis by XT199.

Series no.	Treatment	Branch points[a]	% Inhibition[b]
1	PBS	74 ± 8	
2	FGF	183 ± 11*	
3	FGF+XT199	89 ± 10	86 ± 9

[a]Data represent the means ± SEM, $n = 8$.
[b]As compared with FGF alone.
*$P < 0.001$; for series no. 2, dose level = 1.0 μg/ml; for Series no. 3, dose level = 0.5μg/ml.

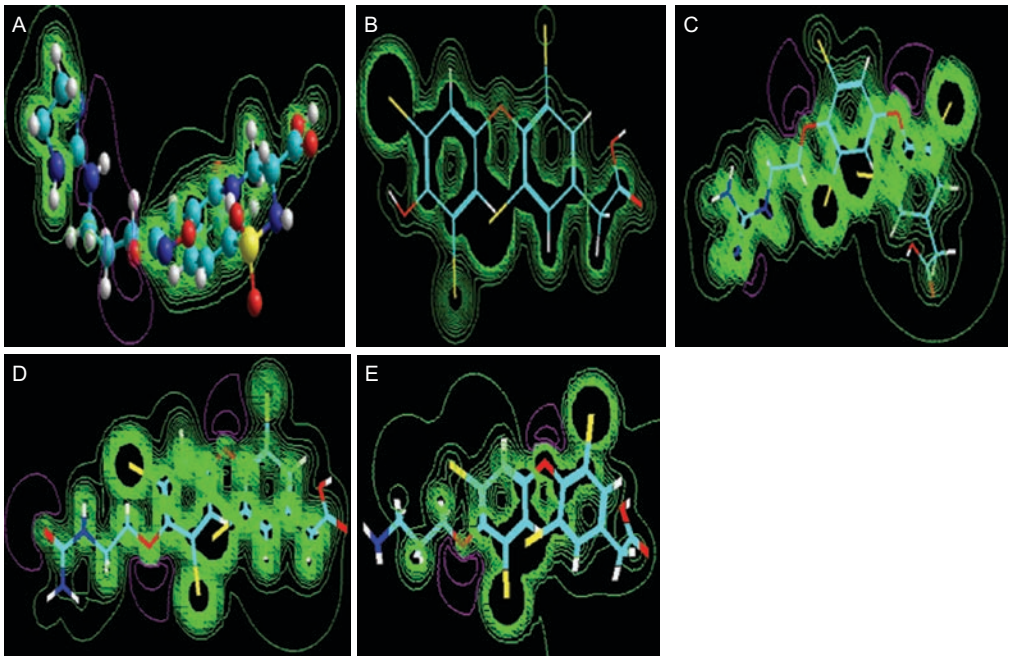

Figure 4. Two-dimensional contour plots of electrostatic potential for XT199 (A), tetrac (B) and compounds (**9**) (C), (**10**) (D) and (**11**) (E).

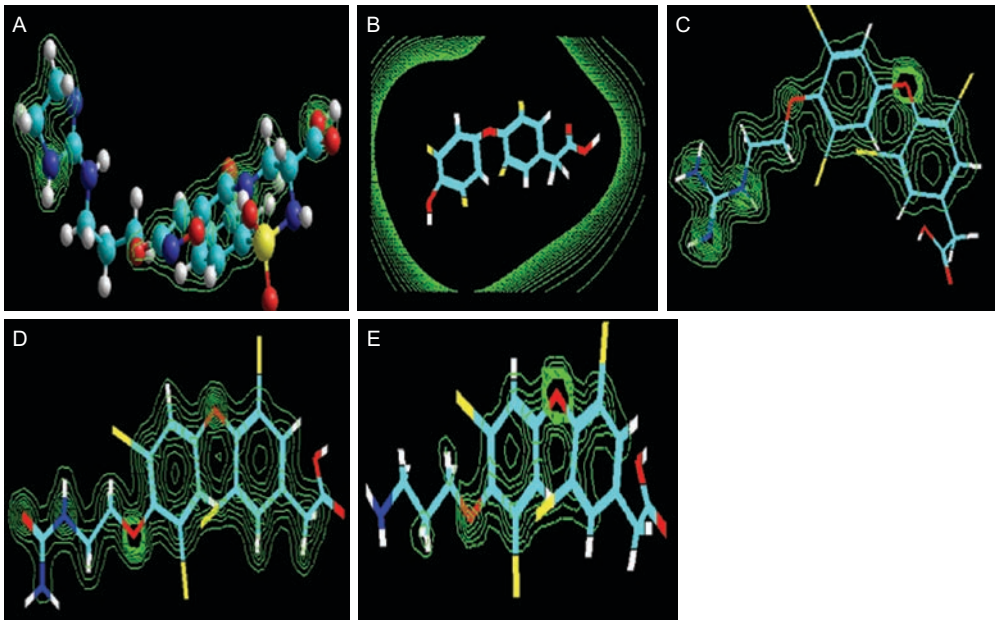

Figure 5. Two-dimensional contour plots of charge density distribution for XT199 (A), tetrac (B) and compounds (**9**) (C), (**10**) (D) and (**11**) (E).

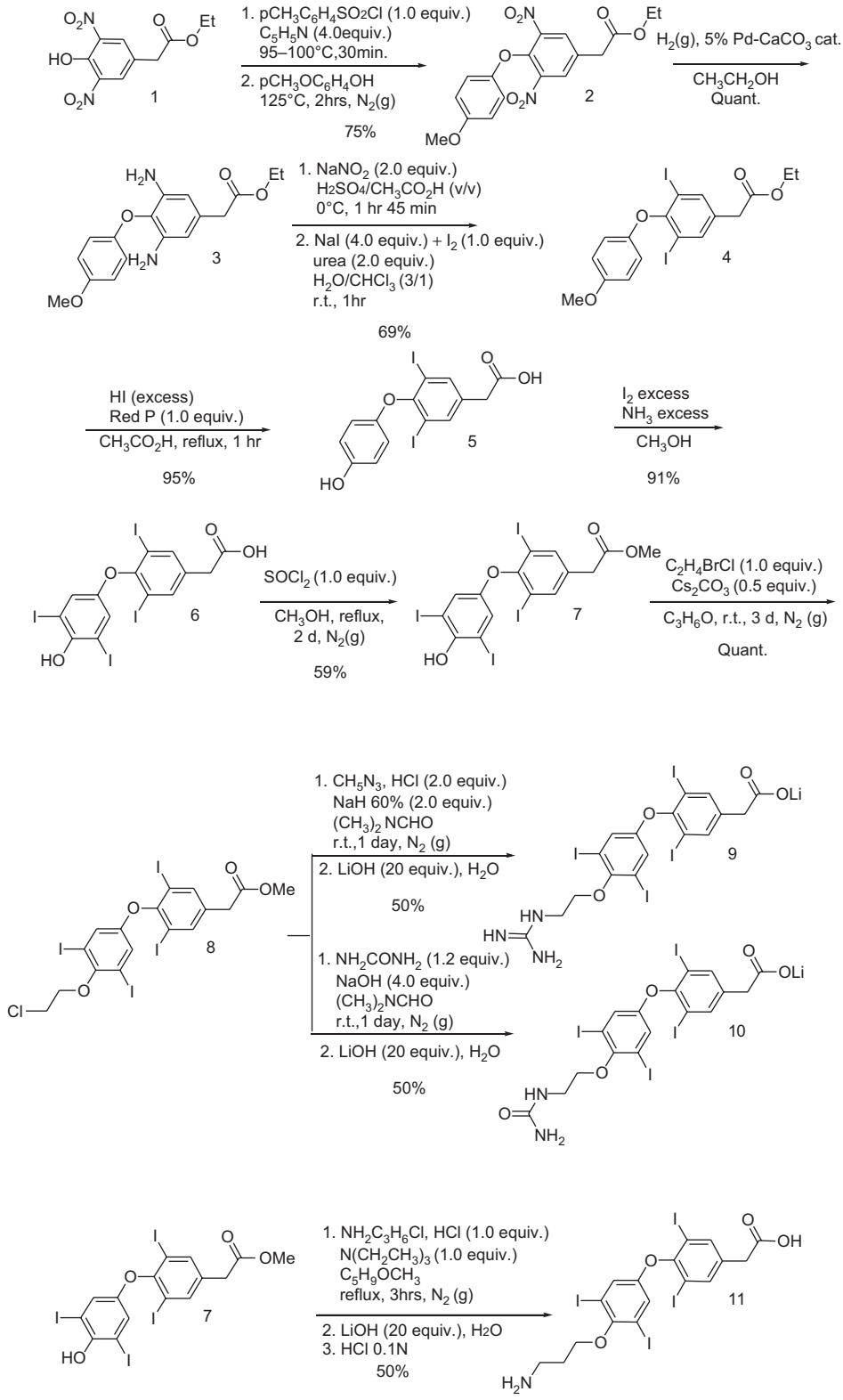

Scheme 1. Preparation of compounds (**9**), (**10**) and (**11**).

and (**11**). Compound (**8**) was reacted with guanidine and urea to yield compounds (**9**) and (**10**), respectively[82,83]. Compound (**11**) was obtained in 47% yield from intermediate (**7**) by refluxing with chloro-propylamine in cyclopentyl-methyl ether as the solvent. Finally, compounds (**9**) and (**10**) were reacted with an excess of aqueous LiOH, while compound (**11**) was reacted with aqueous NaOH to produce the corresponding salts.

The critical step in the synthesis of deiodinated product (**17**) (Supporting Information) was the condensation of compounds (**14**) and (**16**). The bis-aryliodonium triflate (**14**) was prepared from compound (**13**) according

Table 2. Inhibition of angiogenesis by compounds **9**, **10**, and **11**.

Series no.	Treatment	Branch points[a]	% Inhibition[b]
1	PBS	41 ± 5	—
2	FGF	108 ± 8**	—
3	FGF + **tetrac**	57 ± 10	85 ± 14
4	FGF + **9**	65 ± 8	64 ± 13
5	FGF + **9**	58 ± 10	75 ± 16
6	FGF + **10**	56 ± 9	77 ± 13
7	FGF + **10**	58 ± 9	74 ± 13
8	FGF + **11**	55 ± 8	88 ± 11
9	FGF + **11**	66 ± 2	63 ± 3

[a]Data represent means ± SEM, $n = 8$.
[b]As compared with FGF alone.
**$P < 0.001$; for series no. 2, dose level = 2.0 μg/mL; for series nos. 3, 4, 6 and 8, dose = 1.0 μg/mL; for series nos. 5, 7 and 9, dose = 0.25 μg/mL.

to the aryliodonium formation method described by Yokoyama et al.[62]. Compound (**13**) was prepared on both small and high scales by the refluxing methyletherification procedure of 2-isopropylphenol (**12**) using cesium carbonate as a proton trap. In parallel, compound (**16**) was obtained by the methylesterification of commercially available 3,5-di-*tert*-butyl-4-hydroxybenzoic acid (**15**). However, likely due to steric hindrance, the coupling of compounds (**14**) and (**16**) by tetrafluoroborate treatment failed to yield the desired product.

Compounds (**9**), (**10**), and (**11**) exhibited angiogenesis antagonist activity in the CAM model system, with inhibition rates of 63–75% at a dose of 0.25 μg/mL compared with thyroid antagonist XT 199 showing 86% angiogenesis inhibition in same test models at somewhat higher dose levels (Table 2). This dose is not high, considering the designed dual action potency of these characteristically intermediate derivatives of tetrac and XT199. However, these putative dual-action thyrointegrin modulators provide an important tool and foundation for further studies into the extra-cellular biochemical cascades initiated by the thyroid hormone receptor and integrin receptor binding in terms of the signalling pathways activated and the resultant induction of angiogenesis in cancer cells. It is important to note that the interactions predicted by FlexX adhered to strict requirements defined by the patterns exhibited by the αVβ3 antagonists.

Conclusion

Novel dual thyrointegrin modulators were designed and synthesized based on the molecular structures of the thyroid and integrin antagonists. These newly designed compounds have enhanced the understanding of the biological activity of tetrac, a molecule that inhibits tumour growth and metastatic angiogenesis and counteracts resistance to chemotherapy in numerous biological models. Despite the fact that tetrac does not fulfil the requirements for a selective integrin antagonist, it has been observed experimentally to inhibit angiogenesis stimulated by FGF, VEGF, T_4, and T_3. In the current design process, strict molecular requirements for selective binding with integrin αVβ3 were set and then validated compounds were synthesized. The biological activities of these tetrac analogues also indicated that tetrac interaction with αVβ3 integrin, a non-genomic receptor, is not dependent on free phenolic OH groups in the thyroid components.

Declaration of interest

The authors report Vascular Vision Pharmaceuticals Co (VVP Co.) for financial support.

References

1. Giancotti FG, Ruoslahti E. Integrin signaling. Science 1999;285:1028–1032.
2. Schwartz MA. Integrin signaling revisited. Trends Cell Biol 2001;11:466–470.
3. Hynes RO. Integrins: bidirectional, allosteric signaling machines. Cell 2002;110:673–687.
4. Kinbara K, Goldfinger LE, Hansen M, Chou FL, Ginsberg MH. Ras GTPases: integrins' friends or foes? Nat Rev Mol Cell Biol 2003;4:767–776.
5. Boudreau NJ, Jones PL. Extracellular matrix and integrin signalling: the shape of things to come. Biochem J 1999;339 (Pt 3):481–488.
6. Brakebusch C, Fässler R. The integrin-actin connection, an eternal love affair. Embo J 2003;22:2324–2333.
7. Burridge K, Fath K, Kelly T, Nuckolls G, Turner C. Focal adhesions: transmembrane junctions between the extracellular matrix and the cytoskeleton. Annu Rev Cell Biol 1988;4:487–525.
8. Ingber DE. Extracellular matrix as a solid-state regulator in angiogenesis: identification of new targets for anti-cancer therapy. Semin Cancer Biol 1992;3:57–63.
9. Sun HW, Li CJ, Chen HQ, Lin HL, Lv HX, Zhang Y et al. Involvement of integrins, MAPK, and NF-kappaB in regulation of the shear stress-induced MMP-9 expression in endothelial cells. Biochem Biophys Res Commun 2007;353:152–158.
10. Brooks PC, Montgomery AM, Rosenfeld M, Reisfeld RA, Hu T, Klier G et al. Integrin alpha v beta 3 antagonists promote tumor regression by inducing apoptosis of angiogenic blood vessels. Cell 1994;79:1157–1164.
11. Lewis JM, Truong TN, Schwartz MA. Integrins regulate the apoptotic response to DNA damage through modulation of p53. Proc Natl Acad Sci USA 2002;99:3627–3632.
12. Wang XQ, Sun P, Paller AS. Inhibition of integrin-linked kinase/protein kinase B/Akt signaling: mechanism for ganglioside-induced apoptosis. J Biol Chem 2001;276:44504–44511.
13. Giancotti FG. Integrin signaling: specificity and control of cell survival and cell cycle progression. Curr Opin Cell Biol 1997;9:691–700.
14. Zheng DQ, Fornaro M, Bofetiado CJ, Tallini G, Bosari S, Languino LR. Modulation of cell proliferation by the integrin cytoplasmic domain. Kidney Int 1997;51:1434–1440.
15. Watt FM. Role of integrins in regulating epidermal adhesion, growth and differentiation. Embo J 2002;21:3919–3926.
16. Yamada KM, Even-Ram S. Integrin regulation of growth factor receptors. Nat Cell Biol 2002;4:E75–E76.
17. Ruoslahti E, Engvall E. Integrins and vascular extracellular matrix assembly. J Clin Invest 1997;99:1149–1152.
18. Mousa S A, Davis F B, Davis P J. Hormone-integrin cross talk and angiogenesis modulation. Immunol Endocr Metab Agents Med Chem 2009;9:75–83.
19. Gottschalk KE, Günther R, Kessler H. A three-state mechanism of integrin activation and signal transduction for integrin alpha(v) beta(3). Chembiochem 2002;3:470–473.
20. Truong T, Sun G, Doorly M, Wang JY, Schwartz MA. Modulation of DNA damage-induced apoptosis by cell adhesion is

independently mediated by p53 and c-Abl. Proc Natl Acad Sci USA 2003;100:10281–10286.
21. Puigvert JC, Huveneers S, Fredriksson L, op het Veld M, van de Water B, Danen EH. Cross-talk between integrins and oncogenes modulates chemosensitivity. Mol Pharmacol 2009;75:947–955.
22. Brozovic A, Majhen D, Roje V, Mikac N, Jakopec S, Fritz G et al. alpha(v)beta(3) Integrin-mediated drug resistance in human laryngeal carcinoma cells is caused by glutathione-dependent elimination of drug-induced reactive oxidative species. Mol Pharmacol 2008;74:298–306.
23. Luna J, Tobe T, Mousa SA, Reilly TM, Campochiaro PA. Antagonists of integrin alpha v beta 3 inhibit retinal neovascularization in a murine model. Lab Invest 1996;75:563–573.
24. Mousa SA, Mousa AS. Angiogenesis inhibitors: current & future directions. Curr Pharm Des 2004;10:1–9.
25. Wary KK. Molecular targets for anti-angiogenic therapy. Curr Opin Mol Ther 2004;6:54–70.
26. Mousa SA. Anti-integrins as a potential therapeutic target in angiogenesis. Expert Opin Ther Patents 1999;9:1237–1248.
27. Mousa SA. Angiogenesis Inhibitors and Stimulators: Potential Therapeutic Implications. Texas: Landes Bioscience, 2000.
28. Giannis A, Rübsam F. Integrin antagonists and other low molecular weight compounds as inhibitors of angiogenesis: new drugs in cancer therapy. Angew Chem Int Ed Engl 1997;36:588–590.
29. Zitzmann S, Ehemann V, Schwab M. Arginine-glycine-aspartic acid (RGD)-peptide binds to both tumor and tumor-endothelial cells in vivo. Cancer Res 2002;62:5139–5143.
30. Weber WA, Haubner R, Vabuliene E, Kuhnast B, Wester HJ, Schwaiger M. Tumor angiogenesis targeting using imaging agents. Q J Nucl Med 2001;45:179–182.
31. Urbinati C, Mitola S, Tanghetti E, Kumar C, Waltenberger J, Ribatti D et al. Integrin alphavbeta3 as a target for blocking HIV-1 Tat-induced endothelial cell activation *in vitro* and angiogenesis in vivo. Arterioscler Thromb Vasc Biol 2005;25:2315–2320.
32. Temming K, Schiffelers RM, Molema G, Kok RJ. RGD-based strategies for selective delivery of therapeutics and imaging agents to the tumour vasculature. Drug Resist Updat 2005;8:381–402.
33. Ramsden JD. Angiogenesis in the thyroid gland. j Endocrinol 2000;166:475–480.
34. Mousa SA, Bergh JJ, Dier E, Rebbaa A, O'Connor LJ, Yalcin M et al. Tetraiodothyroacetic acid, a small molecule integrin ligand, blocks angiogenesis induced by vascular endothelial growth factor and basic fibroblast growth factor. Angiogenesis 2008;11:183–190.
35. Davis PJ, Davis FB, Lin HY, Mousa SA, Zhou M, Luidens MK. Translational implications of nongenomic actions of thyroid hormone initiated at its integrin receptor. Am J Physiol Endocrinol Metab 2009;297:E1238–E1246.
36. Lei J, Nowbar S, Mariash CN, Ingbar DH. Thyroid hormone stimulates Na-K-ATPase activity and its plasma membrane insertion in rat alveolar epithelial cells. Am J Physiol Lung Cell Mol Physiol 2003;285:L762–L772.
37. Lei J, Mariash CN, Bhargava M, Wattenberg EV, Ingbar DH. T3 increases Na-K-ATPase activity via a MAPK/ERK1/2-dependent pathway in rat adult alveolar epithelial cells. Am J Physiol Lung Cell Mol Physiol 2008;294:L749–L754.
38. Scarlett A, Parsons MP, Hanson PL, Sidhu KK, Milligan TP, Burrin JM. Thyroid hormone stimulation of extracellular signal-regulated kinase and cell proliferation in human osteoblast-like cells is initiated at integrin alphaVbeta3. J Endocrinol 2008;196:509–517.
39. Mousa SA, Davis FB, Mohamed S, Davis PJ, Feng X. Pro-angiogenesis action of thyroid hormone and analogs in a three-dimensional *in vitro* microvascular endothelial sprouting model. Int Angiol 2006;25:407–413.
40. Mousa SA, O'Connor L, Davis FB, Davis PJ. Proangiogenesis action of the thyroid hormone analog 3,5-diiodothyropropionic acid (DITPA) is initiated at the cell surface and is integrin mediated. Endocrinology 2006;147:1602–1607.
41. Yalcin M, Lansing L, Bharali D, Bridoux A, Davis FB, Lin HY, Rebbaa A, Davis PJ, Mousa SA. 79th Annual Meeting of The American Thyroid Association. Chicago, IL: Abstract 110, 2008.
42. Rebbaa A, Chu F, Davis FB, Davis PJ, Mousa SA. Novel function of the thyroid hormone analog tetraiodothyroacetic acid: a cancer chemosensitizing and anti-cancer agent. Angiogenesis 2008;11:269–276.
43. Maas JW, Le Noble FA, Dunselman GA, de Goeij AF, Struyker Boudier HA, Evers JL. The chick embryo chorioallantoic membrane as a model to investigate the angiogenic properties of human endometrium. Gynecol Obstet Invest 1999;48:108–112.
44. Akhtar N, Dickerson EB, Auerbach R. The sponge/Matrigel angiogenesis assay. Angiogenesis 2002;5:75–80.
45. Baffour R, Garb JL, Kaufman J, Berman J, Rhee SW, Norris MA et al. Angiogenic therapy for the chronically ischemic lower limb in a rabbit model. J Surg Res 2000;93:219–229.
46. Mousa SA. Cell adhesion molecules: potential therapeutic & diagnostic implications. Mol Biotechnol 2008;38:33–40.
47. Gadbois DM, Bradbury EM, Lehnert BE. Control of radiation-induced G1 arrest by cell-substratum interactions. Cancer Res 1997;57:1151–1156.
48. Wild-Bode C, Weller M, Rimner A, Dichgans J, Wick W. Sublethal irradiation promotes migration and invasiveness of glioma cells: implications for radiotherapy of human glioblastoma. Cancer Res 2001;61:2744–2750.
49. Lisiak E, Cordes N. Integrins and the cellular radiation response. Cancer Ther 2004;2:271–278.
50. Garcia-Barros M, Paris F, Cordon-Cardo C, Lyden D, Rafii S, Haimovitz-Friedman A et al. Tumor response to radiotherapy regulated by endothelial cell apoptosis. Science 2003;300:1155–1159.
51. Dimitrijevic-Bussod M, Balzaretti-Maggi VS, Gadbois DM. Extracellular matrix and radiation G1 cell cycle arrest in human fibroblasts. Cancer Res 1999;59:4843–4847.
52. Sloan EK, Pouliot N, Stanley KL, Chia J, Moseley JM, Hards DK et al. Tumor-specific expression of alphavbeta3 integrin promotes spontaneous metastasis of breast cancer to bone. Breast Cancer Res 2006;8:R20.
53. Felding-Habermann B, O'Toole TE, Smith JW, Fransvea E, Ruggeri ZM, Ginsberg MH et al. Integrin activation controls metastasis in human breast cancer. Proc Natl Acad Sci USA 2001;98:1853–1858.
54. Cordes N, Meineke V. Cell adhesion-mediated radioresistance (CAM-RR). Extracellular matrix-dependent improvement of cell survival in human tumor and normal cells in vitro. Strahlenther Onkol 2003;179:337–344.
55. Hallahan D, Geng L, Qu S, Scarfone C, Giorgio T, Donnelly E et al. Integrin-mediated targeting of drug delivery to irradiated tumor blood vessels. Cancer Cell 2003;3:63–74.
56. Damiano JS, Cress AE, Hazlehurst LA, Shtil AA, Dalton WS. Cell adhesion mediated drug resistance (CAM-DR): role of integrins and resistance to apoptosis in human myeloma cell lines. Blood 1999;93:1658–1667.
57. Gardiner EJ, Willett P, Artymiuk PJ. Graph-theoretic techniques for macromolecular docking. J Chem Inf Comput Sci 2000;40:273–279.
58. Moitessier N, Henry C, Maigret B, Chapleur Y. Combining pharmacophore search, automated docking, and molecular dynamics simulations as a novel strategy for flexible docking. Proof of concept: docking of arginine-glycine-aspartic acid-like compounds into the alphavbeta3 binding site. j Med Chem 2004;47:4178–4187.
59. Cody V, Davis PJ, Davis FB. Molecular modeling of the thyroid hormone interactions with alpha v beta 3 integrin. Steroids 2007;72:165–170.
60. Wilkinson JH. Synthesis of some possible metabolites of thyroxine and triiodothyronine. Biochem j 1956;63:601–605.
61. Baxter JD, Goede P, Apriletti JW, West BL, Feng W, Mellstrom K et al. Structure-based design and synthesis of a thyroid hormone receptor (TR) antagonist. Endocrinology 2002;143:517–524.
62. Yokoyama N, Walker GN, Main AJ, Stanton JL, Morrissey MM, Boehm C et al. Synthesis and structure-activity relationships of oxamic acid and acetic acid derivatives related to L-thyronine. J Med Chem 1995;38:695–707.

63. Xiong JP, Stehle T, Goodman SL, Arnaout MA. New insights into the structural basis of integrin activation. Blood 2003;102:1155–1159.
64. Xiong JP, Stehle T, Zhang R, Joachimiak A, Frech M, Goodman SL et al. Crystal structure of the extracellular segment of integrin alpha Vbeta3 in complex with an Arg-Gly-Asp ligand. Science 2002;296:151–155.
65. Marinelli L, Lavecchia A, Gottschalk KE, Novellino E, Kessler H. Docking studies on alphavbeta3 integrin ligands: pharmacophore refinement and implications for drug design. J Med Chem 2003;46:4393–4404.
66. Henry C, Moitessier N, Chapleur Y. Vitronectin receptor alpha(V) beta(3) integrin antagonists: chemical and structural requirements for activity and selectivity. Mini Rev Med Chem 2002;2:531–542.
67. Mousa SA. alphav Vitronectin receptors in vascular-mediated disorders. Med Res Rev 2003;23:190–199.
68. Mousa SA. Anti-integrin as novel drug-discovery targets: potential therapeutic and diagnostic implications. Curr Opin Chem Biol 2002;6:534–541.
69. Mousa SA. Angiogenesis promoters and inhibitors: potential therapeutic implications. Mol Med Today 1996;2:140–142.
70. Kerr JS, Slee AM, Mousa SA. The alpha v integrin antagonists as novel anticancer agents: an update. Expert Opin Investig Drugs 2002;11:1765–1774.
71. Bridoux A, Cui H, Dyskin E, Yalcin M, Mousa SA. Semisynthesis and pharmacological activities of Tetrac analogs: angiogenesis modulators. Bioorg Med Chem Lett 2009;19:3259–3263.
72. Davis FB, Mousa SA, O'Connor L, Mohamed S, Lin HY, Cao HJ et al. Proangiogenic action of thyroid hormone is fibroblast growth factor-dependent and is initiated at the cell surface. Circ Res 2004;94:1500–1506.
73. Bergh JJ, Lin HY, Lansing L, Mohamed SN, Davis FB, Mousa S et al. Integrin alphaVbeta3 contains a cell surface receptor site for thyroid hormone that is linked to activation of mitogen-activated protein kinase and induction of angiogenesis. Endocrinology 2005;146:2864–2871.
74. Davis PJ, Davis FB, Cody V. Membrane receptors mediating thyroid hormone action. Trends Endocrinol Metab 2005;16:429–435.
75. Tucker GC. Inhibitors of integrins. Curr Opin Pharmacol 2002;2:394–402.
76. Tucker GC. Alpha v integrin inhibitors and cancer therapy. Curr Opin Investig Drugs 2003;4:722–731.
77. Crater WdeC. Nitration. Ind Eng Chem 1951;43:1987–1990.
78. Clugston M, Flemming R (eds). Advanced Chemistry (Advanced Science). USA: Oxford University Press, 2000, p. 326.
79. Skinner HF. Metamphetamine synthesis via hydriodic acid/red phosphorus reduction of ephedrine. Forensic Sci Int 1990;48:123–134.
80. McCullagh JV, Daggett KA. Synthesis of triarylmethane and xanthenes dyes using electrophilic aromatic substitution reactions. J Chem Educ 2007;84:1799.
81. Vaidyanathan G, Shankar S, Affleck DJ, Alston K, Norman J, Welsh P et al. Meta-iodobenzylguanidine derivatives containing a second guanidine moiety. Bioorg Med Chem 2004;12:1649–1656.
82. Sham HL, Zhao C, Stewart KD, Betebenner DA, Lin S, Park CH et al. A novel, picomolar inhibitor of human immunodeficiency virus type 1 protease. J Med Chem 1996;39:392–397.